Effect of stress-relief anneal time on residual stress of Co-Cr-Mo parts manufactured with selective laser melting

Genevieve Rousseau[1*], *Jaundrie* Fourie[1], *CP* Kloppers[1], and *Deon* Marais[2]

[1]North-West University, Department of Additive Manufacturing, Potchefstroom, South Africa
[2]The South African Nuclear Energy Corporation (Necsa) SOC Limited, Research and Innovation Division, Pretoria, South Africa

Abstract. Thermal inconsistencies inherent in the selective laser melting manufacturing process generate residual stress that may exceed the yield strength of the material resulting in deformation and cracking of components. This may however be mitigated through a stress-relief annealing process. The purpose of this study is to investigate the effect of stress-relief anneal time on the residual stress in selective laser melted Co-Cr-Mo components by means of simulation and neutron diffraction techniques. Thin-walled samples were manufactured and subjected to heat treatment at 1065ºC for different holding times (0.25, 1, 2 and 3 hours) as well as a sample heat treated at 750ºC for 1 hour. Evaluation of the residual stress reveals that the heat-treated samples have significantly lower residual stress as compared to an as-built (non-heat treated) control sample. Results indicate that the range of annealing times investigated produce near-identical residual stress values. Higher annealing temperatures however result in lower residual stresses. Comparison of simulated and neutron diffraction results indicate anisotropic behaviour of the material which can be attributed to the layer-wise addition of material.

1 Introduction

Cobalt-Chrome-Molybdenum (Co-Cr-Mo) alloys are used extensively in the medical and dental fields due to their outstanding biocompatibility, mechanical properties, wear and corrosion resistance [1, 2]. Dental components have historically been manufactured in dental laboratories using a casting method similar to the lost-wax process. This method is time consuming and relies on skilled and experienced technicians [3]. Selective laser melting (SLM) is an additive manufacturing (AM) technique that has gained interest as an alternative manufacturing method for Co-Cr-Mo dental components due to its ability to rapidly manufacture complex geometries [4-6]. SLM has improved significantly over years of research and offers the possibility to produce parts with near 100% density [7]. One of the disadvantages of the SLM process is the build-up of residual stress within the printed parts

* Corresponding author: rousseau.genevievenwu@gmail.com

due to thermal gradients experienced during the manufacturing process. Heat treatment is commonly used to minimize the residual stress and is known as stress-relief anneal [8].

Several studies have investigated the effect of stress-relief annealing on the microstructure and mechanical properties of additively manufactured metal components. It is shown that stress-relief annealing Co-Cr-Mo at temperatures above 1050 ºC significantly improves the ductility of printed parts and decreases the likelihood of deformation and cracking after removal from the build plate. Studies used varying annealing times ranging from 15 minutes to 6 hours [9-15]. Szala et al. investigated the effect of stress-relief annealing hold time on the microstructure and hardness coefficients of 42CrMo4 steel. The result indicated that all the annealing processes tested, resulted in microstructural evolution from lamellar cementite to granular and semi-lamellar morphology. The spheroidized microstructure facilitated in microstructural softening and effectively decreased the Vickers hardness. The shortest tested holding time of 15min resulted in the lowest Vickers hardness and it was therefore concluded that the holding time can be minimized whilst facilitating microstructure softening and decreasing hardness coefficients [15]. Additional studies are however required to fully understand the influence of stress-relief annealing hold time on the residual stress. In this current study, Co-Cr-Mo samples were manufactured by the SLM process and the residual stresses in the samples were investigated in the as-built condition and after heat treatment. The SLM process was also modelled using the Simufact Additive (SAS) package [16]. The aim of the study was to make use of simulation software and neutron diffraction (ND) techniques to demonstrate the effect of selected stress-relief annealing time on residual stress in SLM Co-Cr-Mo samples.

2 Material and methods

2.1 Sample preparation

The material used throughout the study is medical grade Co-Cr-Mo alloy manufactured by Praxair with the chemical composition complying with the ASTM F75 standard as shown in Table 1[17, 18] with an average powder-particle size of 27 microns. Samples with dimensions and shown in Fig. 1 were manufactured using an ORLAS Creator SLM machine [19] with laser power, speed and layer height set at 170 W, 600 mm/s and 0.025 mm respectively. During the SLM process the build chamber was continuously purged with nitrogen to prevent oxidation.

Table 1. Chemical composition of Co-Cr-Mo alloy powder in mass % specified by ASTM F75 [17].

	Co	**Cr**	**Mo**	**Ni**	**C**	**Fe**	**Si**	**Mn**
TruForm CoCr (Co-538)	Balance	27-30	5-7	<0.25	<0.35	<0.75	<1	<1

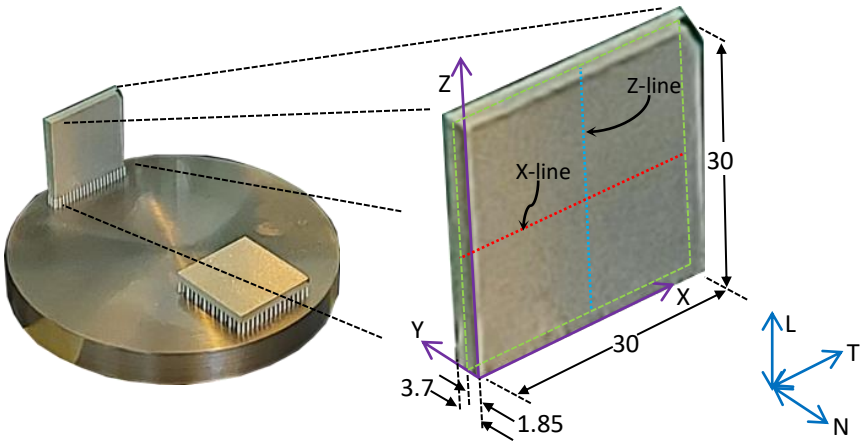

Fig. 1. Sample dimensions (in mm) and reference coordinate systems.

Literature indicates that heat treatment temperatures between 900°C and 1150°C ensure sufficient residual stress relief and enhanced mechanical properties [14, 15]. Electro Optical Systems (EOS) suggests a final heat treatment hold temperature of 750°C for one hour [18]. In addition to this strategy, four other holding times at 1065°C as well as an as built (no heat treatment) control sample, were investigated as summarised in Table 2.

Table 2. Heat treatment strategies investigated.

Sample number	**0**	**1**	**2**	**3**	**4**	**5**
Temperature [°C]	N/A	1065	1065	1065	1065	750
Hold time [min]	N/A	15	60	120	180	60

2.2 Neutron Diffraction

The experimental neutron work was conducted with the Materials Probe for Internal Strain Investigation (MPISI) angular dispersive neutron diffractometer located at the South African Fundamental Atomic Research Installation 1 (SAFARI-1) nuclear research reactor. MPISI was configured to deliver a monochromatic neutron beam with a wavelength (λ) of 1.64734(7) Å [20]. A nominal gauge volume (GV) of 2 × 2 × 2 mm^3 was established by the width and height of the incident beam aperture, as well as the width of the diffraction-side aperture. Neutrons diffracting from the (311) crystallographic plane of the sample were captured by the area detector with its centre positioned at a $2\theta_{detector}$ angle of 99.52°.

The nominal GV resulted in an instrumental gauge volume (IGV) shown in Fig. 2(a), as determined by step-scanning a calibration pin through the beam intersection and fitting an appropriate analytic function to the resulting neutron intensity distribution. The IGV side length of 2.25 mm at an angle of 99.52° implies that the closest measurement to the surface ensuring a fully submerged IGV is 1.71 mm. Measurements taken closer than this from the sample surface will experience partial GV illumination resulting in pseudo strains which may influence the result if not accounted for. In order to eliminate the need for partial GV correction, only fully embedded ND measurements in the central plane (where Y=1.85 mm) at locations as indicated in Fig. 2(b) were considered.

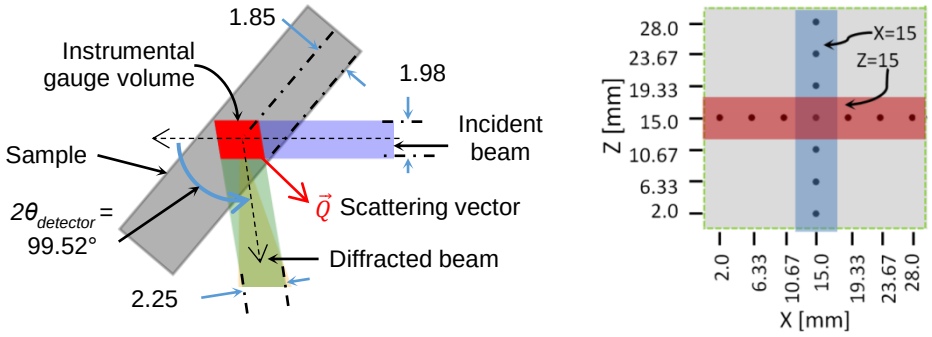

(a) *(b)*

Fig. 2. (a) Top view schematic of ND implementation and (b) measurement positions.

After flat field and geometric correction, the Debye-Scherrer ring was integrated and the peak position ($2\theta_{311}$) determined from the least-squares fitting of a Voigt profile function. The positional fitting error represents the uncertainty in measurements. Bragg's law, given in Eq. 1, was used to determine the lattice spacing (d_{hkl}) corresponding to the diffraction angle at each measurement position.

$$n\lambda = 2d_{hkl}sin\theta_{hkl} \tag{1}$$

The variation in the strained lattice plane spacing (d^i_{hkl}) with reference to the strain-free lattice plane spacing ($d_{0,hkl}$) was used to calculate the directional elastic lattice strain (ε^i_{hkl}) in the material using Eq. 2. The scattering vector ($\vec{Q}$) is defined by the bisect of the incident and diffracted beams, therefore by re-orientating and re-positioning the sample, the different position dependent *i*-components i.e. transverse (T), longitudinal (L) and normal (N), as depicted in Fig. 3 can be obtained. Subsequently, the tri-axial residual stress was calculated using the generalized form of Hooke's law as given by Eq. 3.

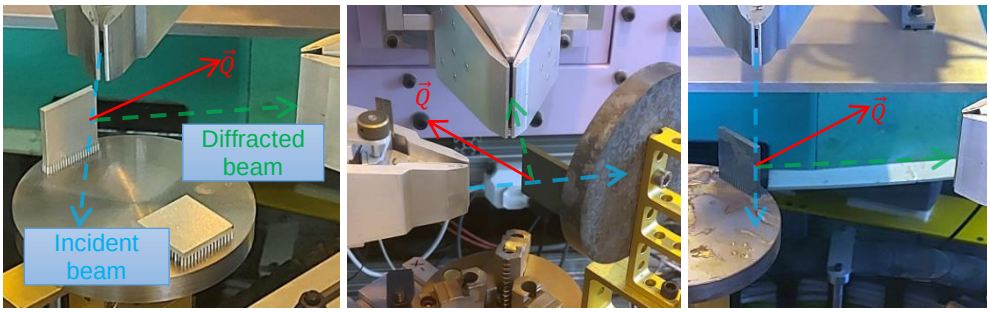

(a) *(b)* *(c)*

Fig. 3. Experimental setups for measuring (a) transverse (b) longitudinal and (c) normal strain components

$$\varepsilon^i_{hkl} = \frac{d^i_{hkl} - d_{0,hkl}}{d_{0,hkl}} \tag{2}$$

$$\sigma^i_{hkl} = \frac{E}{1-\nu}\varepsilon^i_{hkl} + \frac{\nu E}{(1+\nu)(1-\nu)}(\varepsilon^L_{hkl} + \varepsilon^N_{hkl} + \varepsilon^T_{hkl}) \tag{3}$$

The strain-free lattice plane spacing was determined by applying the bi-axial stress condition ($\sigma_{hkl}^{N} = 0$) as applicable to thin-walled samples to Eq. 3 resulting in Eq. 4. This assumption simplifies the experimental requirements [22, 23].

$$d_{0,hkl} = \frac{d_{hkl}^{N} + \left(\frac{1}{2}s_2 + 2s_1\right) - s_1(d_{hkl}^{L} + d_{hkl}^{T})}{\frac{1}{2}s_2} \quad (4)$$

The material properties and constants used for this study are given in Table 3 and were determined from $CoCr_{20}Mo_{10}$ alloy which has similar composition as ASTM F75 [24, 25].

Table 3. Material properties and constants used for ND calculations.

	Lattice plane (hkl)	**s_1 [MPa^{-1} × 10^{-6}]**	**½ s_2 [MPa^{-1} × 10^{-6}]**	**E [GPa]**	**ν [-]**
$CoCr_{20}Mo_{10}$	(311)	-1.70984	6.891192	193	0.33

2.3 Simulation

The residual stress induced as a result of the additive manufacturing process was simulated using the SAS package. SAS offers three calculation methods for simulating the SLM process: mechanical; thermal; and thermo-mechanical [16, 26-28]. These calculation methods can be used to determine the final shape of the component after residual stresses have caused deformation; detect hot spots and possible errors due to lack of fusion; examine the final microstructure; and digitally apply and test process parameters before manufacturing.

The mechanical calculation method uses the inherent strain method to give insight into distortion behaviour and internal stresses. The thermal calculation method gives insight into thermal processes such as peak temperatures. The thermo-mechanical calculation method combines the mechanical and thermal calculations to give full insight into the SLM process. For this study the thermo-mechanical calibration method was used firstly requiring mechanical, thermal and thermo-mechanical calibration. The initial inherent strain values were determined through mechanical calibration and the optimized exposed energy fraction (EEF) through the thermal calibration. EEF is the ratio between the fraction of energy that melts the powder and the fraction of energy that dissipates into other layers. The thermo-mechanical calibration is used to calculate the volumetric expansion factor (VEF) and all variables determined through the calibration processes are used in the final simulation to ensure highest accuracy results.

The mechanical calibration requires manufacturing cantilever beams with the material and print parameters for which the inherent strains are required. The cantilever beams are partially cut and the residual stress induced distortion is measured, as presented in Fig. 4. The software uses the difference between the experimentally determined maximum z-height ($z_{i,exp}$) and the simulated maximum z-height ($z_{i,sim}$) at point *i* to estimate the inherent strain values (ε) by applying the least squares method where *n* is the number of samples, presented with Eq. 5.

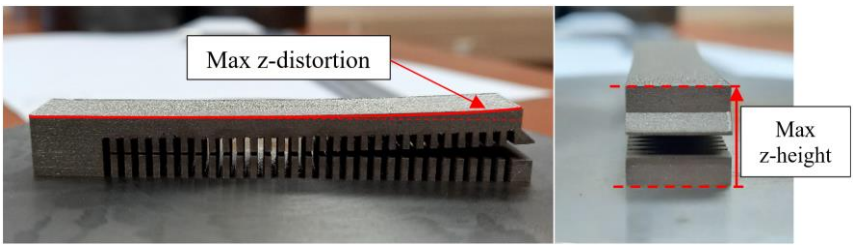

Fig. 4. Mechanical calibration cutting and measuring method.

$$\varepsilon = \sum_{i=1}^{n} \left(z_{i,exp} - z_{i,sim}\right)^2 \quad (5)$$

The thermal calibration is performed with the same material, print parameters and cantilever geometry as used for the mechanical calibration. The software estimates the peak temperature that the sample experiences during manufacturing and determines the EEF. The thermo-mechanical calibration uses the EEF value as an input and varies the VEF until the required z-distortion, as determined in the mechanical calibration, is reached. The inherent strain, EEF and VEF is used in all consecutive simulations to ensure highest accuracy results.

The simulation process is summarised in Table 5. The material and process parameters are constant and identical to the calibrations. All steps are repeated for each heat treatment strategy with variation in heat treatment hold time. The generated mesh is shown in Fig. 5.

Table 4. Simulation process

Step	Process description	Detail
1	Setup simulation main process properties	Simulation configuration: thermo-mechanical Type of simulation: manufacturing Manufacturing process stages: build and heat treat
2	Define machine properties	Build space: 250 × 250 × 200 mm Base plate: circular Machine parameters: maximum laser power set at 250 W
3	Specify base plate design parameters	Thickness: 13 mm Material: Inconel 718
4	Choose powder material	Material selection: CoCr_powder based on EOS Cobalt Chrome MP1
5	Import sample geometry	Sample geometry: stl. File type import Positioning: centre and 4mm z-offset from base plate
6	Generate support structure	Method: Simufact Support radius: 0.35 mm Support distance: 0.185 mm
7	Input build properties	Heat flux: input EEF and VEF values as determined by calibration Chamber initial temperature: 25°C Base plate initial temperature: 25°C
8	Define heat treatment parameters	Approach: transient heat treatment Time-temperature table: input specific heat treatment strategy
9	Generate the mesh	Mesh type: Non-uniform Levels of coarsening: 0 Voxel size:0.4375x0.5x0.5 mm
10	Run the analysis	Start analysis Voxel results: export arc. file type
11	Extract results from exported file	Simufact Arc Tool: extract data to txt. file format Excel: copy relevant output values to Microsoft Excel for further processing

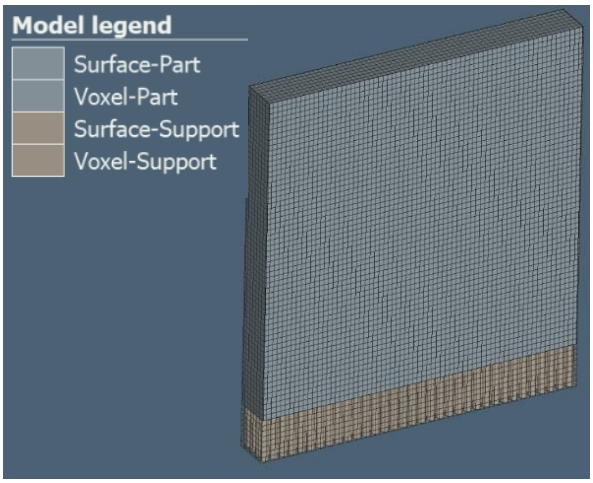

Fig. 5. Simufact Additive generated mesh.

3 Results and discussion

The SAS analysis resulted in 33493 data points for each sample and the tri-axial stresses were extracted at all nodal positions. The ND IGV of 2.25 × 1.98 × 2.0 mm^3 was considered and the data points within this volume integrated to obtain values that can be directly compared with the ND results. Table 5 shows the ND data compared to SAS results for all measurement positions in each principal stress direction (T, N and L) as well as the hydrostatic stress. The results for the SAS are presented by solid lines with the sample number prefixed with 'S'. The ND results are represented by dashed lines with the sample number prefixed with 'N'.

Table 5. Comparison of simulated and measured tri-axial residual stresses.

	X-Line	Z-Line
		
Normal	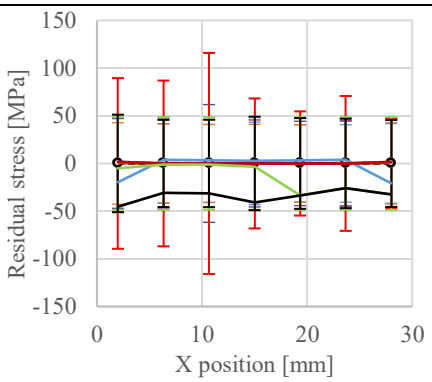	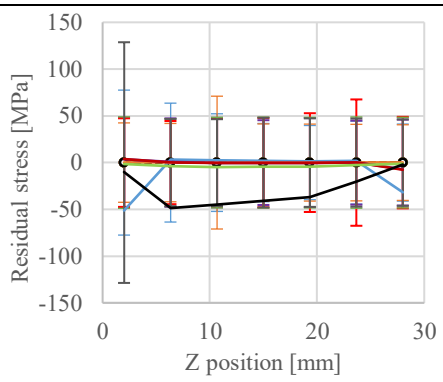
Longitudinal	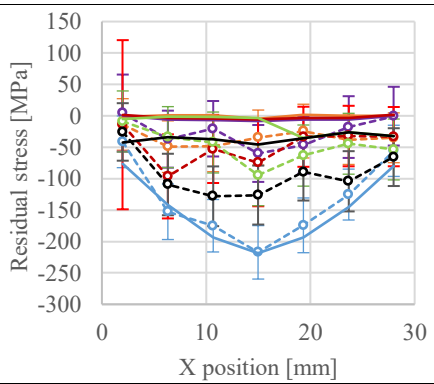	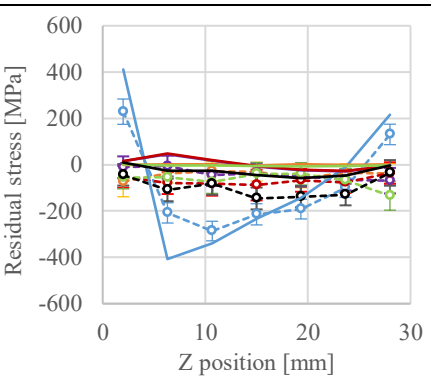
Transverse	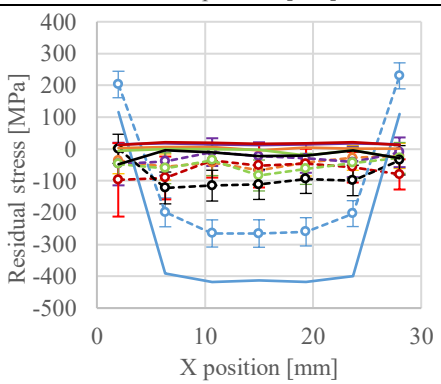	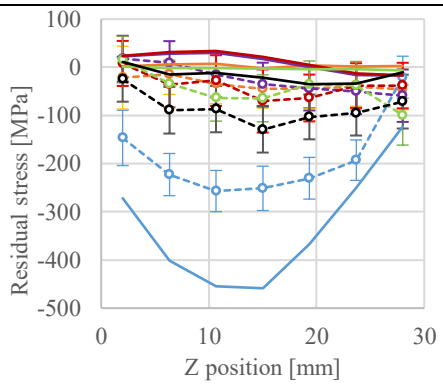

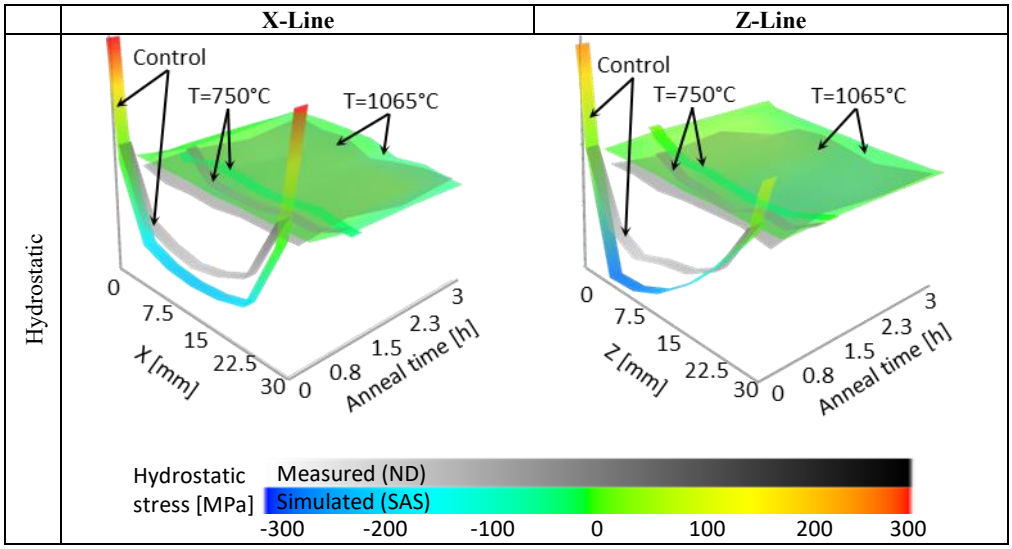

Using N0 as a baseline the difference between N0 residual stress and the heat-treated sample results was calculated to gauge the effect that each heat treatment strategy had on the residual stress relief, as presented in Table 6 and Table 7**.**

Table 6. Difference between N0 and each heat treatment strategy for the Longitudinal data.

	Position [mm]	2	6.33	10.67	15	19.33	23.67	28	**Average [MPa]**
X Position	**N1**	239.1	142.5	222.6	198.7	218.4	175.2	251.7	206.9
	N2	250.1	160.2	255.6	242.6	230.4	162.3	240.3	**220.2**
	N3	299.8	108.0	229.6	213.8	214.0	145.6	309.9	217.3
	N4	249.8	138.7	230.2	182.4	197.8	159.5	257.9	202.3
	N5	202.2	76.6	150.3	154.4	166.4	104.2	265.4	159.9
Y Position	**N1**	125.0	208.4	222.4	207.0	186.3	152.3	25.2	160.9
	N2	164.4	231.9	241.7	216.0	186.3	142.5	38.5	**174.5**
	N3	154.5	187.0	229.4	181.3	166.7	154.9	17.4	155.9
	N4	162.5	188.9	193.6	186.9	195.1	154.6	78.8	165.8
	N5	121.8	133.6	170.1	122.0	127.3	98.0	50.7	117.6

Table 7. Difference between N0 and each heat treatment strategy for the Transverse.

	Position [mm]	2	6.33	10.67	15	19.33	23.67	28	**Average [MPa]**
X Position	**N1**	27.6	103.5	126.8	182.6	150.0	87.3	20.8	99.8
	N2	45.7	115.5	154.4	157.4	127.7	107.4	55.2	**109.0**
	N3	27.2	56.2	122.2	142.9	141.0	93.1	22.6	86.5
	N4	32.4	118.8	132.5	122.9	111.0	80.9	2.1	85.8
	N5	15.7	43.3	46.9	91.1	85.1	21.1	10.0	44.8
Y Position	**N1**	301.7	170.7	258.2	184.2	133.1	63.0	168.3	**182.7**
	N2	240.2	202.0	241.6	176.7	142.6	34.9	199.7	176.8
	N3	281.0	128.8	205.7	126.4	124.0	23.5	166.7	150.9
	N4	284.9	153.0	211.0	174.7	152.2	32.1	264.5	181.8
	N5	272.6	99.0	204.0	68.5	53.6	29.4	166.1	127.6

Analysis off the Normal stresses shows close correlation of all data points. SAS indicated residual stress values no larger than 50 MPa which falls within the uncertainty associated with the ND data. This residual stress is determined to be negligible. The simulation result also supports the bi-axial stress condition imposed on the ND measurements for calculating reference $d_{0,hkl}$ values.

Analysis of the Longitudinal and Transverse data indicates overall close correlation except for the Transverse component of the control sample where the SAS simulation over predicts the residual stress. The SAS analysis shows results for residual stress relief under ideal conditions with isotropic material properties such as Youngs' modulus. The simulation does not account for variation in the printing procedure such as powder particle size, powder distribution on the build plate, heat flux variation during heat treatment, daily temperature affecting the heat treatment cooling rate, variation in furnace heating rate and microstructural defects within the material which may affect the results.

The Longitudinal stress relief results seen in Table 6 indicated that N2 was the best performing heat treatment strategy with and average of 220.2 MPa and 174.5 MPa at the X and Y positions respectively. The largest average difference between the samples heat treated at 1065°C was 18.6 MPa which was a clear indication that the heat treatment holding time had very little overall influence on the residual stress relief. The most noticeable difference in average stress relief was for N5 with the lowest overall average of 159.9 MPa and 117.6 MPa at the X and Y positions respectively.

The Transverse stress relief results seen in Table 7 indicated that N2 was the best performing heat treatment strategy at the X position with an average of 109.0 MPa and N1 was the best performing heat treatment strategy at the Y position with an average of 182.7 MPa. The largest average difference between the samples heat treated at 1065°C was 31.9 MPa. Although this was a much larger difference compared to the Longitudinal stress it was still within the uncertainty associated with the ND data and indicated that the heat treatment holding time had little overall influence on the residual stress relief. The most noticeable difference in average stress relief was again for N5 with the lowest overall average of 44.8 MPa and 127.6 MPa at the X and Y positions respectively.

Analysis of the Longitudinal and Transverse stress relief results indicate that the heat treatment temperature had a bigger influence on the average residual stress relief than the heat treatment holding time.

4 Conclusion

The samples that were heat treated at 1065 °C showed a higher degree of residual stress relief than the 750 °C treated sample. The results indicate that residual stress relief occurs in a shorter time frame than anticipated, and that heat treatments consisting of holding time longer than 15 minutes do not yield improved results at the elevated temperature investigated. Comparison of the SAS and ND results indicate a close correlation between data sets when the experimental uncertainty is considered. The larger deviation between ND and SAS results observed in the transverse stress may be attributed to increased anisotropic behaviour of AM components. Due to the layer-by-layer addition of material the thermal gradient and anisotropic material properties is more prevalent. This study concludes that the stress-relief annealing hold time does not have a significant influence on the extent of residual stress relief in AM components. It may therefore be beneficial to decrease traditional stress relief anneal hold time when only considering residual stress.

The mechanical properties of AM Co-Cr-Mo heat treated to 1065 °C for 15 min should be studied to determine the validity of this heat treatment strategy for use in the AM post-processing of dental components.

References

1. L. Hitzler et al., Adv. Mater. Sci., **2018** (2018) doi: 10.1155/2018/8213023.
2. B. Konieczny, A. Szczesio-Wlodarczyk, J. Sokolowski, K. Bociong, Materials, **13**, 16 (2020) doi: 10.3390/ma13163524.
3. S. Bhatia, K. Ramadurai, *3D printing and bio-based materials in global health* (2017)
4. T. Narushima, K. Ueda, A. Alfirano, *Co-Cr Alloys as Effective Metallic Biomaterials*, in Biomaterials Science and Engineering (2015). doi: 10.1007/978-3-662-46836-4_7.
5. M. Canciglieri, A. Leite, A. Szejka, O. Canciglieri Júnior, Int. J. Comput. Integr. Manuf. **32**, 9 (2019). doi: 10.1080/0951192x.2019.1636410.
6. A. Wijk, I. Wijk, *3D printing with biomaterials* (2015)
7. A. Ovsianikov, J. Yoo, V. Mironov, *3D Printing and Biofabrication*, (2020)
8. X. Wang, K. Chou, J. Manuf. Process. **48** (2019). doi: 10.1016/j.jmapro.2019.10.027.
9. W. Lee, J. Wang, C. Hsu, P. Peng, J. Prosthet. Dent. (2020). doi: 10.1016/j.prosdent.2020.06.038.
10. S. L. Sing, W. Y. Yeong, *Effect of heat treatment on cobalt-chromium-molybdenum alloy fabricated by selective laser melting*, in Proc. of the 3rd Int. Conf. on Progress in Additive Manufacturing, Nanyang Technological University (2018). doi: 10.25341/D4NP43
11. K. Mantrala, M. Das, V. Balla, C. Rao, V. Kesava Rao, Front. Mech. Eng. **1** (2015). doi: 10.3389/fmech.2015.00002.
12. W. Wei et al., Metall Mater Trans A **51** 6 (2020). doi: 10.1007/s11661-020-05719-y.
13. X. Yan, H. Lin, Y. Wu, W. Bai, J. Prosthet. Dent. **119**, 6 (2018). doi: 10.1016/j.prosdent.2018.04.002.
14. Y. Kajima et al., Mater. Sci. Eng. A **726** (2018). doi: 10.1016/j.msea.2018.04.048.
15. M. Szala, G. Winiarski, Ł. Wójcik, T. Bulzak, Materials **13**, 9 (2020). doi: 10.3390/ma13092022.
16. Simufact Engineering, Simufact Additive: Technology. [Online]. Available: https://www.simufact.com/technology.html
17. Specification for Cobalt-28 Chromium-6 Molybdenum Alloy Castings and Casting Alloy for Surgical Implants (UNS R30075), F04 Committee, West Conshohocken, PA.
18. Electro Optical Systems, EOS CobaltChrome SP2 for EOSINT M 270. [Online]. Available: https://www.stratasysdirect.com/-/media/files/direct/material-datasheets/direct-metal-laser-sintering/dmls_cobalt_chrome_sp2_material_specifications.pdf
19. OR Laser ORLAS CREATOR review - hybrid metal 3D printer, Aniwaa. Available: https://www.aniwaa.com/product/3d-printers/or-laser-orlas-creator/#:~:text=The%20OR%20Laser%20ORLAS%20CREATOR.
20. A. Venter, *Activities at Safari-1 research reactor on residual stress measurements* International Atomic Energy Agency (IAEA) (2005).
21. A. Venter, P. van Heerden, D. Marais, J. Raaths, Physica B Condens. Matter **551** (2018). doi: 10.1016/j.physb.2017.12.011.
22. M. Ripley, Mater. Forum **30** (2006)
23. S. Goel et al., Mater. Des **195** (2020). doi: 10.1016/j.matdes.2020.109045.

24. M. Sedighi, R. Nazemnezhad, Exp. Tech. **40**, 1(2016). doi: 10.1007/s40799-016-0033-9.
25. I. C. Noyan, J. B. Cohen, *Residual stress: measurement by diffraction and interpretation* (1987).
26. Simufact - Manufacturing Process Simulation for Metalworking Industry, MSC Software, (2021). [Online]. Available: https://www.mscsoftware.com/product/simufact.
27. Simufact Engineering, Introducing the inherent strain method: Tutorial. Accessed: (2021).
28. T. Taufek, Y. Manurung, S. Lüder, M. Graf , F. Salleh, *Distortion Analysis of SLM Product of SS316L using Inherent Strain Method*, in Proceedings of the IOP Conference Series: Materials Science and Engineering, **834**, 1 (2020). doi: 10.1088/1757-899x/834/1/012011.